Title

A tissue-mimicking prostate phantom for 980 nm laser interstitial thermal therapy

Journal

International Journal of Hyperthermia, 36(1)

ISSN

0265-6736

Authors

Geoghegan, R
Santamaria, A
Priester, A
et al.

Publication Date

2019

DOI

10.1080/02656736.2019.1660811

HHS Public Access

Author manuscript

Int J Hyperthermia. Author manuscript; available in PMC 2020 January 01.

Published in final edited form as:

Int J Hyperthermia. 2019 ; 36(1): 993–1002. doi:10.1080/02656736.2019.1660811.

A Tissue-Mimicking Prostate Phantom for 980nm Laser Interstitial Thermal Therapy

R. Geoghegan[1], **A. Santamaria**[2], **A. Priester**[1,2], **L. Zhang**[3], **H. Wu**[1,3], **W. Grundfest**[1], **L. Marks**[2], **S. Natarajan**[1,2]

[1]Department of Bioengineering, University of California, Los Angeles, CA 90095

[2]Department of Urology, University of California, Los Angeles, CA 90095

[3]Department of Radiological Sciences, University of California, Los Angeles, CA 90095

Abstract

Purpose: To develop a phantom with optical and thermal properties matched to human prostate. This phantom will provide a platform for the development and characterization of 980nm laser interstitial thermal therapy (LITT) systems.

Methods: A polyacrylamide gel was doped with Naphthol Green B, Intralipid, and Bovine Serum Albumin (BSA). The necessary concentration of each ingredient was determined by measuring the optical properties via fluence measurements and light diffusion theory. LITT was then performed under the same conditions as a previous clinical trial in which temperature was monitored via a thermal probe. The thermal data and induced coagulation zone were compared to clinical data to illustrate the similarity between the phantom and patient. LITT was also performed under magnetic resonance thermometry (MRT).

Results: The requisite concentrations of Naphthol Green B, Intralipid and BSA were found to be 0.144% (w/v), 8.06% (v/v) and 31.4% (v/v) respectively. In the native state, the absorption coefficient and reduced scattering coefficient (μ_s') were found to be 0.66 ± 0.06 cm^{-1} and 8.27 ± 0.50 cm^{-1} respectively, with μ_s' increasing to 17.63 ± 1.41 cm^{-1} after coagulation. The thermal response of the phantom was similar to that observed clinically with maximum thermal probe measurements of 64.2°C and 66.9°C respectively. The shape of the induced coagulation zone was qualitatively and quantitatively similar to the MRT zone of elevated temperature and the coagulation zone observed clinically.

Conclusions: A phantom which simulates optical and thermal response to 980nm LITT was constructed and demonstrated to be similar to human prostate.

Keywords

laser ablation; tissue phantom; prostate; optical properties

Introduction

Laser interstitial thermal therapy (LITT), also known as focal laser ablation (FLA), has been demonstrated to be a promising method of focal therapy for prostate cancer [1–4]. The

procedure consists of inserting a laser fiber into a target tumor and raising the temperature above 60°C. A 980nm diode laser is frequently used. Given the fixed wavelength, the induced zone of coagulative necrosis is primarily dependent on laser power, exposure duration and device characteristics such as diffuser length. Understanding the effect of these parameters on the resulting damage zone is critical for clinical success. Prior work investigating thermal response has relied on animal models [5–7] and cadaveric prostate [8]. Such models are heterogeneous across specimens, resulting in the requirement for a large number of samples to accurately assess laser-tissue interaction. The optical properties of these models may not be sufficiently similar to human prostate and the experimental approach is complicated by their biohazardous nature. Additionally, the zone of thermal necrosis is difficult to quantify and requires histologic analysis. Therefore, there is a need to develop a tissue-mimicking phantom to provide a standardized, controllable model for investigations of both the optical and thermal response of prostatic tissue to 980nm LITT.

Magnetic resonance thermometry (MRT) is frequently used as a method of monitoring LITT; however, the resulting damage maps have been shown to overestimate the extent of thermal necrosis due to motion artifact and inaccurate thermal damage models [9]. Interstitial thermal probes have also been used as a method for monitoring ablation [10,11]. In contrast to MRT, interstitial probes only provide thermal data for a single point. It is therefore necessary to utilize *a priori* assumptions to estimate the volume of coagulative necrosis. A tissue-mimicking phantom would provide a robust platform for further development of both MRT and interstitial thermal probes in this field. In this work we have developed the requisite phantom and demonstrated similarity to prostatic tissue using previously acquired clinical data. Furthermore, it is envisioned that the phantom will find utility in the development and characterization of LITT systems as well as for validation of computational models.

The propagation of light in tissue is governed by the absorption coefficient (μ_a) and the reduced scattering coefficient (μ_s'). The reduced scattering coefficient is given by $\mu_s' = \mu_s(1 - g)$, where μ_s and g are the scattering coefficient and anisotropy factor respectively. In order to achieve clinically relevant thermal damage volumes in a phantom, the material must possess both a similar μ_a and μ_s' to tissue. Moreover, studies have shown that thermal tissue damage can cause up to a five-fold increase in total attenuation [12–14]. This is predominantly due to increased scatter as a result of thermally induced protein coagulation. The phantom material must therefore, also exhibit dynamic optical properties such that μ_s' increases substantially when exposed to temperatures sufficient to induce rapid protein coagulation. This threshold is generally accepted to be 60°C [15]. Studies have highlighted the correlation between optical properties and the resulting coagulation zone during LITT. For example, using an *in vivo* murine model, Nikfarjam et al. found that an Nd-Yag (1064nm) laser takes 50s to achieve the same coagulation zone diameter as observed after 20s with a diode laser (980nm) [16]. This occurs because the diode laser has a shorter penetration depth. Similar results were reported by Jiang et al. through simulation of LITT in the liver [17]. After 600s the predicted volume of coagulated tissue was almost three times greater using a 980nm (native: μ_a=0.6cm^{-1}, μ_s' = 9.7cm^{-1}, coagulated: μ_a=0.5cm^{-1},

μ_s' = 14.7cm^{-1}) laser compared to a 1064nm (native: μ_a=0.3cm^{-1}, μ_s' = 9.0cm^{-1}, coagulated: μ_a=0.2cm^{-1}, μ_s' = 13.9cm^{-1}) laser.

Both thermal conductivity and specific heat capacity also play an important role in determining the final ablation volume. It is difficult to manipulate these properties without altering the material's optical properties; however, most phantoms are composed primarily of water which has similar thermal properties to tissue. Finally, the thermal damage volume must be observable post-ablation. This can be achieved by sectioning the phantom and quantifying the thermal damage under direct visualization. It is also advantageous to observe the damage volume without disturbing the material via ultrasound or MRI.

Many tissue-mimicking phantoms have been proposed for the analysis of thermal therapy. Negussie et al. reported on a polyacrylamide gel doped with thermochromic ink [18] with color changes correlated with temperature increase. They also demonstrated that the phantom exhibited thermal properties similar to human soft tissue. Zhang et al. developed a similar phantom in which the damage zone was visualized through the coagulation of BSA [19]. BSA is optically transparent in its native state but opaque when coagulated. This phantom was based on prior work by McDonald et al. who demonstrated that the coagulation temperature of BSA can be altered by controlling pH [20]. Without altering the pH, BSA coagulates in polyacrylamide phantoms at 70°C [21] which is considerably higher than observed during LITT. McDonald et al. also demonstrated that the coagulation zone can be quantified with T_2-weighted magnetic resonance imaging (MRI). This was possible in that phantom due to the thermal response of the protein in the BSA. Thermally-induced protein aggregation hinders the rotational averaging of protein dipolar interactions, thus; protein-proton transverse relaxation time is reduced resulting in contrast between native and coagulated states [22]. T_1-weighted imaging may also be used; however, the T_1 relaxation times for proteins are very long and are not as heavily impacted by protein aggregation.

While all of these phantoms are useful for analyzing thermal damage, none of them have been demonstrated to possess optical properties similar to human tissue and thus they are not suitable for the analysis of LITT. In contrast, Iizuka et al. demonstrated a method for quantifying phantom optical properties and designed an albumin and agar phantom with similar optical properties to human tissue at 805nm [23]. The albumin is a key ingredient as it ensures an increase in μ_s' during LITT. In this paper we use the same method as Iizuka et al. for quantifying phantom optical properties to develop a tissue-mimicking prostate phantom for LITT at 980nm. While the optical properties of prostatic tissue may vary between patients and even within the same patient, we sought to achieve an μ_a and μ_s' of 0.66cm^{-1} and 8.1cm^{-1} respectively as these values have been reported for human prostate at 980nm [24]. To our knowledge these are the only published values for μ_a and μ_s' at 980nm in human prostate; however, they are consistent with other studies in the near-infrared region [13,25]. In addition, the coagulation-induced increase in scatter in the human prostate has been reported to range from 71-130% in the near-infrared region [13,25]. As a result, we elected to design the phantom with a 100% coagulation-induced increase in $\mu_s'(\Delta\mu_s')$

In contrast to Iizuka et al., we utilized a polyacrylamide gel doped with BSA to ensure that the coagulation temperature can be adjusted using the pH method demonstrated by McDonald et al. We then demonstrate that the thermal response of the phantom can be measured via interstitial thermal probes and MRT. Quantification of the coagulation zone was demonstrated non-invasively using T_2-weighted MRI and via direct visualization after sectioning. Finally, we compared our results with data previously acquired in a clinical trial in which LITT was used for the treatment of prostate cancer [11].

Methods

Phantom Construction

Polyacrylamide gel was chosen as the base material for the phantom due to its high melting point, optical transparency, and appropriate thermal properties [18]. The gel was prepared by mixing Acrylamide/bis-acrylamide (19:1 40% w/v, Thermo Fisher Scientific Inc., CA, AM9024) with degassed deionized water. The solution was then doped with various ingredients to change the phantom optical properties. At 980nm, the primary absorbers in tissue are water molecules, oxyhemoglobin and deoxyhemoglobin. As polyacrylamide contains a large quantity of water, the μ_a of the base material is close to that of prostatic tissue. To match μ_a to prostatic tissue, Naphthol Green B (Sigma-Aldrich, MI, N7257-100G) was used as it is readily absorbed in water; thus, resulting in minimal scatter. In contrast Intralipid (20% v/v, Fresenius Kabi, Sweden) was used to increase μ_s' as it is an effective scatterer and a weak absorber. Moreover, Intralipid preferentially scatters light in the forward direction; therefore, phantoms doped with Intralipid will possess g values similar to soft tissue [26]. Intralipid is a solution of soybean oil (20%), egg yolk phospholipids (1.2%), glycerin (2.25%) and water (76.55%). Phospholipid micelles from the soybean oil scatter light; thus, μ_s' can be altered by varying Intralipid concentration [27]. Finally, BSA (30.8% w/v, Boval Co., TX, CF-0020) was used to ensure an increase in μ_s' post ablation while also providing contrast for MRI and direct visualization.

To reduce the coagulation temperature of BSA to 60°C, a 0.2M citrate buffer was added to ensure a pH ~ 4.7. The buffer consists of citric acid anhydrous (Sigma-Aldrich, MI, C0759) and sodium citrate tribasic dehydrate (Sigma-Aldrich, MI, S4641). Further details on this method can be found in McDonald et al. [20]. To prevent bubbles from appearing in the phantom, the BSA was thoroughly degassed and added after all other ingredients were dissolved in water. Since the polymerization reaction is exothermic, and could cause premature BSA coagulation, the solution was chilled (4-8°C) before adding the initiator. Due to the reduced pH, the widely used combination of TEMED and ammonium persulfate could not be used to initiate polymerization. Instead, polymerization was initiated via a combination of L-ascorbic acid (Sigma-Aldrich, MI, A5960), iron (II) sulfate heptahydrate (Sigma-Aldrich, MI, F7002) and hydrogen peroxide (30% w/v, Sigma-Aldrich, MI, H1009) as previously used by McDonald et al. [20]. The solution was then immediately poured into 70mm x 70mm x 40mm thin walled (1mm) prefabricated molds, sealed and refrigerated. Table 1 shows the recipe for a 1L phantom without altering the optical properties by addition of Naphthol Green B, Intralipid or BSA. Throughout this paper, the increase in volume due

to the addition of BSA and/or Intralipid addition was offset by a corresponding reduction in water volume; hence, the total volume remained constant.

Absorption Coefficient as Function of Naphthol Green B Concentration

Naphthol Green B was identified as an appropriate dye to increase the absorption coefficient as it is a known absorber at 980nm. Solutions of Naphthol Green B (0.05%-0.4% w/v) dissolved in water were tested to ensure that LITT would not bleach the dye or otherwise alter μ_a. 7ml of each solution was placed in a test-tube and a 600μm core laser fiber with a 15mm long diffuser (Medtronic, Dublin, Ireland) was inserted into the center of the tube. Each sample was then exposed to 980nm light at 13.75W for 3 minutes. These parameters were chosen to match those used in a previously conducted clinical trial of prostate cancer LITT to enable comparison with *in vivo* patient data [11]. A spectrophotometer (Agilent 8453 UV-visible Spectroscopy System) was used to measure the absorbance (A) of each solution before and after exposure to the laser light. By assuming negligible scatter, μ_a was calculated using the following formula which can be derived from Beer's Law [28]:

$$\mu_a = ln\,(\frac{100}{\%T})d \qquad \text{(Eqn. 1)}$$

where %T is the percentage of light transmitted ($A=2-\log_{10}\%T$) and d is the thickness of the cuvette (1cm).

Phantoms doped with increasing concentrations of Naphthol Green B (0%, 0.05%, 0.15%, 0.25% and 0.35% w/v) were manufactured to determine its relationship with μ_a using the above method. Five samples of each concentration were prepared by adding Naphthol Green B to the recipe outlined in Table 1. It was anticipated that the initiator, hydrogen peroxide, would bleach the dye; therefore, measurements were made in the polyacrylamide phantom rather than in a dye and water solution. The phantoms were prepared from 20ml solutions, 3ml of which was placed in a cuvette immediately after the addition of the initiator. The cuvettes were then covered and refrigerated. To assess the bleaching effect, the μ_a was determined for each sample at 24 hrs, 48 hrs and 72 hrs.

Method of Measuring the Reduced Scattering Coefficient

The apparatus shown in Figure 1 was used to measure the μ_s' as previously demonstrated by Iizuka et al. [23]. In contrast to Iizuka et al., measurements were taken after polymerization. It consists of a 3D printed testing chamber, a point source probe (Pioneer Optics, Bloomfield, CT) connected to a 980nm diode laser (Photex Inc, Houston, TX), a micrometer-controlled translation stage (Thorlabs, Newton, NJ) and a dosimetry probe (Pioneer Optics, Bloomfield, CT) connected to an amplified photodetector (PDA36A, Thorlabs, Newton, NJ). Using custom-built software and a microcontroller (Arduino Leonardo, Arduino LLC, Italy), the PHOTOVOLTAGE (V) was recorded every 500μm as the dosimetry probe was advanced towards the source probe. These data were then used to calculate the effective attenuation (μ_{eff}) coefficient as the fluence rate (ϕ) for an isotropic point source radiator is given by [28]:

$$\phi(r) \propto \frac{exp\,(-\mu_{eff}r)}{r} \quad \text{(Eqn. 2)}$$

where r is the distance between the source and detector. Given that $V \propto \phi$, the magnitude of the slope of ln $(V \cdot r)$ vs r is the μ_{eff}. As μ_a is known, the μ_s' can then be determined using the following definition of μ_{eff} [28]:

$$\mu_{eff} = \sqrt{3\mu_a \cdot (\mu_a + \mu_s')} \quad \text{(Eqn. 3)}$$

The apparatus was calibrated against a spectrophotometer using a non-scattering medium as there was no material with a known μ_s' available. Briefly, 300ml phantoms doped with Naphthol Green B (0-0.35%) were manufactured and poured into custom designed 3D printed boxes prior to polymerization. 3ml of each solution was also placed in cuvettes for spectrophotometric analysis. μ_{eff} was determined from absorbance using Eqn. 1, Eqn. 2 and assuming that $\mu_a \gg \mu_s'$. A standard 2-point calibration was then performed using the phantoms with 0% and 0.35% Naphthol Green B.

Reduced Scattering Coefficient as a Function of BSA & Intralipid Concentration

Phantoms doped with 0.144% (w/v) Naphthol Green B (derived optimal concentration) and 12.5%, 25% and 37.5% (v/v) BSA were manufactured in triplicate. The phantoms were cast in thin walled containers with openings to facilitate two measurements in the fluence box apparatus (Fig. 1). The two measurement sites are separated by 23mm which is sufficient to ensure that an existing needle track will not affect the second measurement. Due to the bleaching effect previously observed, testing was performed ~48hrs after initiation of polymerization. The μ_s' was determined for each phantom at room temperature. The phantoms were then placed in plastic bags to prevent water absorption and submerged in a water bath for 2hrs at 70°C. This was found to be sufficient to raise the temperature of the entire phantom above 65°C; thus, ensuring coagulation throughout the volume. The μ_s' was then quantified again using a different section of the phantom. The optimal concentration of BSA was defined as the concentration that results in $\Delta\mu_s'$ of 8.1cm^{-1} (a 100% increase).

BSA causes minimal scatter in its native state, thus the addition of Intralipid was required to achieve the desired μ_s' of 8.1 cm^{-1} in the native state. A second set of phantoms was manufactured in triplicate containing 0.144% Naphthol Green B (derived optimal concentration), 31.4% BSA (derived optimal concentration) and increasing concentrations of Intralipid (0%, 5%, 10%). The μ_s' was determined in the native and coagulated states following the same protocol outlined for the BSA only phantoms.

Testing Optimized Phantom

The derived phantom recipe was used to create eight optimized phantoms. Five of these phantoms were used to determine μ_s' in the native and coagulated states following the same

protocol as used previously. The remaining three phantoms were tested to assess the thermal response under the same conditions previously used in a clinical trial [11]. The trial utilized components from an existing magnetic resonance-guided laser ablation system (Medtronic, Dublin, Ireland) along with magnetic resonance - ultrasound fusion guidance via the Artemis® device (Eigen, Grass Valley, California). The key components were a 15W 980nm laser (BioTex, Houston, Texas), a 600 μm core laser fiber (Medtronic, Dublin, Ireland), K-pump surgical infusion pump (K.M.I., Corona, California), Uro-kit 600 dual lumen catheter (Medtronic, Dublin, Ireland), Fluoroptic® thermal probes (Lumasense, Santa Clara, California) and a custom-fabricated needle guide. Figure 2A depicts the clinical setup in which the laser fiber housed in a saline cooled dual lumen catheter was inserted into the target. The procedure was monitored via a thermal probe placed level with the catheter tip and at a radial distance of 8mm. Figure 2B elucidates the phantom experimental setup designed to match the clinical procedure. The experiment utilizes the same laser fiber, dual lumen catheter, infusion pump and thermal probe. Component placement was achieved using a custom-fabricated insulated box with needle tracks placed 8mm apart. Prior to being placed in the box, phantom temperature was raised to 37± 1°C using a water bath. LITT was performed for 3 min. at 13.75 W, matching parameters of the clinical trial. In contrast to the clinical trial, the experiment was simultaneously monitored via gradient echo magnetic resonance thermometry to demonstrate the utility of the phantom for the development of MRT sequences.

Measurement of the coagulation zone was then demonstrated using MRI and direct visualization. Immediately after laser deactivation, a high resolution T_2-weighted turbo spin echo image was acquired (echo time = 52ms, repetition time = 2000ms, resolution = $0.5*0.5*1mm^3$) using a 3T scanner (Prisma, Siemens). Alignment of the imaging plane with the fiber trajectory was achieved using a fiducial marker within the insulated box. The fiducial marker consisted of a 2x2mm water-filled channel circumscribing the phantom. Following laser application, the phantom was sliced in half along the fiber trajectory and photographed.

Results

Absorption Coefficient

The effect of photobleaching was examined by comparing μ_a before and after LITT in Naphthol Green B and water solutions (Fig. 3). The difference in μ_a was found to be negligible at all concentrations (mean absolute error = 0.035 cm^{-1}); therefore, it can be assumed that Naphthol Green B will not photobleach during LITT. In polyacrylamide phantoms, a non-linear relationship was observed between Naphthol Green B concentration and μ_a (Fig. 4). This was previously observed by Iizuka et al. [23], who attributed this effect to bleaching induced by the initiator, ammonium persulfate (APS). They found that bleaching only occurs during the first 2 hours after the addition of APS. In contrast, hydrogen peroxide was used as the initiator in our phantoms and appears to cause bleaching beyond 24hrs. No further bleaching was observed after 48 hours. The requisite concentration of Naphthol Green B to achieve the desired μ_a of 0.66 cm^{-1} was determined by interpolating

the data from the 48hr and 72hr measurements. It was found that 0.144% Naphthol Green B results in an μ_a of 0.66 ± 0.06 cm^{-1}.

Reduced Scattering Coefficient

Prior to determining the reduced scattering coefficient, the fluence box was calibrated against a spectrophotometer. μ_{eff} measured by the fluence box was linear ($r^2 = 0.998$) throughout the measurement range. After standard 2-point calibration was applied, μ_{eff} measured by the fluence box and spectrophotometer was equivalent (mean absolute error = 0.033 cm^{-1}).

Figure 5A shows the data measured by the fluence box in order to calculate μ_s' for a set of phantoms doped with various concentrations of BSA before and after coagulation. The slope of the curves gives μ_{eff} which was used to generate Fig. 5B as previously described (Eqn. 2). Figure 6 shows the corresponding curves for phantoms doped with the optimal concentration of BSA and increasing concentrations of Intralipid. All measurements were taken at least 48 hours after adding the initiator to ensure that the bleaching effect had subsided. As expected, the presence of BSA ensures a coagulation-induced increase in μ_s' with 31.4% BSA providing the desired $\Delta\mu_s'$ of 8.1 cm^{-1}. In the native state the target μ_s' is also 8.1 cm^{-1} which is achieved by adding 8.06% Intralipid. Interestingly, Intralipid also appears to have some effect on the coagulation-induced increase in μ_s'.

Incorporating optimized concentrations for BSA and Intralipid yielded a final phantom recipe (Table 2) which was subsequently characterized in the same manner as before (Fig. 7). The optical properties are summarized in Table 3. The mean $\Delta\mu_s'$ across the five tested samples was 113±11%.

Thermal Response

Figure 8 compares the thermal response of the phantom to a patient under the same conditions. The temperature was recorded at radial distance of 8mm from the laser fiber in both cases. After 180s, the laser was deactivated and the maximum temperature was found to be 64.1±0.9°C and 66.9°C in the phantom and patient respectively. The temperature dropped rapidly following laser deactivation, reaching 60°C in 10s and 44±5s for the patient and phantom respectively.

Figure 9(A–C) demonstrates the utility of the phantom as a robust platform for the development of MRT sequences for monitoring LITT. Thermal maps were calculated from phase maps acquired during the procedure. The zone of elevated temperature was localized around the laser fiber as expected. The growth of this zone was evident as the procedure progressed. Additionally, the maximum temperature recorded in each of the three phantoms was 98.8°C, 99.2°C and 99.7°C.

LITT Induced Coagulation

Figure 10 compares the induced coagulation zone in (A) a patient, (B) a phantom under T_2-weighted MRI, and (C) a phantom under direct visualization. The experiment was performed

on three phantoms and in all cases the coagulation zone approximates an ellipse. The major and minor axes for the phantom were 2.65±0.03cm and 1.6±0.05cm on MRI and 2.58±0.03cm and 1.52±0.01cm under direct visualization. A similar coagulation zone was observed clinically with major and minor axes of 2.44cm and 1.51cm respectively.

Discussion

We have developed a novel tissue-mimicking phantom with similar optical and thermal properties to human prostatic tissue. The relationship between phantom ingredients and optical properties was determined empirically using fluence measurements and light diffusion theory. In the native state μ_a and μ_s' have been reported as 0.66cm^{-1} and 8.1cm^{-1} in human prostate at 980nm [24]. In addition, LITT causes coagulative necrosis leading to an increase in μ_s' which is expected to lie in the range of 71-130% [13,25]. To mimic these properties the requisite concentrations of Naphthol Green B, Intralipid and BSA were quantified and found to be 0.144%, 31.4% and 8.06% respectively which resulted in μ_a and μ_s' of 0.66±0.06cm^{-1} and 8.27±0.5cm^{-1} in the native state. After coagulation μ_s' , increased to 17.63±1.41 which corresponds to an increase of 113%. The phantom optical properties therefore correspond to the expected values of prostatic tissue at 980nm. In addition, the phantom coagulation threshold was matched to tissue (~60°C) by reducing pH to 4.7 as outlined in a previous study [20].

The measured change in μ_s' after coagulation is higher than predicted as we assumed that the coagulation-induced increase in μ_s' was solely due to BSA protein coagulation and independent of Intralipid. This assumption was found to be incorrect as the presence of Intralipid led to a relatively small increase in the coagulation induced change in μ_s'. This was not anticipated but may be due to interaction between the two substances. Indeed, earlier studies have shown that fatty acid alters the BSA denaturation process [29,30]. Moreover, in our calculations we have assumed that μ_a remains constant during laser exposure. While we demonstrated that this is true for the absorbing agent Naphthol Green B, when dissolved in water, it is possible that interactions with other ingredients results in an alteration of μ_a. This is unlikely as it has previously been demonstrated that the effect of dyes dissolved in water on μ_a is independent of scattering introduced by Intralipid [31–33]. While the assumption is frequently made when designing tissue mimicking phantoms, it could be verified using alternative techniques such as the inverse adding doubling method [34]. Nevertheless, the measured increase in μ_s' is similar to previously reported values for prostatic tissue in the near-infrared region [13,25]. In the limited number of human prostate samples studied, the maximum coagulation-induced increase in μ_s' was 130%, while 272% was reported for canine studies with a much larger sample size.

It should also be noted that in contrast to a previous study by Iizuka et al. [23], we were able to measure the optical properties after polymerization; thus, chemical reactions with the initiator have been accounted for. This greatly reduces measurement uncertainty as the initiator contains hydrogen peroxide which bleaches Naphthol Green B resulting in a decrease in μ_a after polymerization. For some studies it may be desirable to increase the

BSA content in an effort to achieve a greater post-coagulation increase in μ_s'. While this is possible, we limited BSA concentration to 37.5%, as higher concentrations resulted in the formation of large bubbles.

The thermal response of the phantom was compared to previously acquired clinical data. The maximum temperature observed clinically was 66.9°C while the phantom peaked at 64.2±0.9°C at the same location. Interestingly, after laser deactivation, the temperature drops to 60°C, the theorized damage threshold, 44s earlier in the patient. Given this relatively short timeframe it is likely that there is only a minor increase in coagulation volume as minimal damage occurs during the cooling phase [35]. This variation in the rate of cooling is likely due to the absence of perfusion in the phantom as well as possible disparity in active cooling. Perfusion has been shown to affect both the volume of thermal damage and the temperature distribution during LITT [36]. In addition, further active cooling is provided by continuous circulation of water through the dual lumen catheter; however, the flow rate and temperature were not precisely controlled. Positioning of the thermal probe was also a challenge in the clinical setting. A needle guide was used to aid in placement; however, the needle was susceptible to deflection when passing through the prostatic tissue. Additionally, in the clinical study, the distal section of the thermal probe was covered with a thin copper film to prevent laser light from interfering with the thermal measurement. This occurs as the thermal probe relies on fluoroptic technology in which the temperature is determined based on the decay rate of a phosphor element at the tip of the probe. The decay rate is assessed using a photodiode sensitive to 980nm light. In our MRI experiments the copper film was removed and an in-line filter was used to remove the offending light. This approach was taken as the copper film would likely cause an artifact on MRI. The absence of the copper film may also explain the initial rapid heating observed in the phantom as light can be absorbed directly by the Tefzel jacket covering the thermal probe. Likewise, the rate of cooling in the clinical setting may have been faster as the copper film rapidly conducts heat away from the sensor tip after laser deactivation.

We also demonstrated that the thermal response during LITT can be monitored via MRT as shown in previous clinical trials [2,3]. The data from the MRT images facilitates analysis of the thermal response throughout a single plane. At the end of LITT, data from the MRT images shows that the temperature near the fiber is approximately 100°C with a maximum temperature of 99.7°C. This was expected and correlates with clinical experience in which char is frequently observed on the dual lumen catheter after removal. Despite the high temperatures, the phantom does not appear to melt. While we did not measure the melting point, a previous study found the melting point of similar polyacrylamide phantoms to be 113°C [37].

Finally, the LITT-induced coagulation zone was compared to that found clinically. In the phantom, the induced coagulation zone was readily apparent under T_2-weighted MRI and direct visualization after sectioning along the laser fiber trajectory. It was found to be quantitively and qualitatively similar to the non-perfused region observed on a contrast-enhanced MRI acquired immediately after a patient received LITT for the treatment of prostate cancer. Moreover, the MRT derived temperature map acquired during LITT of the

phantom (Fig. 9[Fig. 9) appears to correlate with the coagulation zone identified in both the patient and phantom (Fig. 10). This suggests that the phantom provides a useful platform for studying the effect of procedure parameters on the resulting coagulation zone and also for development of feedback techniques including MRT.

The advantages of this phantom over *ex vivo* tissue are numerous. It is homogenous, reproducible, and easy to work with as it is not a biohazard, unlike cadaveric tissue. It should be noted that acrylamide monomers are toxic; therefore, safety procedures must be adhered to during fabrication. After polymerization the risk is substantially reduced; however, nitrile gloves should still be worn due to the possibility of residual monomers. A key advantage of this phantom is the ability to accurately quantify the coagulation zone. This can be achieved via either direct visualization or T_2-weighted MRI. Given this characteristic, the phantom should find utility in both the development and characterization of laser interstitial thermal therapy systems. Finally, the thermal and optical properties of the phantom are similar to human prostate; thus, the phantom provides a useful platform for the development of monitoring modalities such as magnetic resonance thermometry and interstitial thermal probes.

Like many other phantoms a lack of perfusion is the primary limitation of this model; therefore, this phantom is likely to find utility as a substitute for *ex vivo* rather than *in vivo* studies. In addition, the phantom does not account for *in vivo* factors such as the urethra, prostate capsule, prostate stones or capsular cooling. Consequently, the phantom should not be used for direct pre-treatment planning. It should also be noted, that while every effort was made to match the phantom's optical properties to human prostate, batch to batch variation in the optical properties of Naphthol Green B, Intralipid and BSA was not considered in our analysis. This potential variation is likely to be minor and have a limited impact on the phantom's thermal response. Finally, knowledge of g and μ_a are important for Monte Carlo modelling but could not be determined due to the employed method of measuring the optical properties. This limitation can be overcome by assuming g=0.74 as previously reported for Intralipid [26]. This assumption must be utilized with some caution as the effect of BSA coagulation on g is unknown.

To our knowledge this is the first phantom with all of the following characteristics: (1) optical properties matched to bulk prostatic tissue at 980nm, (2) thermal response similar to clinical data, and (3) visualization of the induced damage zone via MRI and direct visualization. These characteristics make this phantom ideal for the development and characterization of tools for laser interstitial thermal therapy at 980nm.

Conclusion

A tissue mimicking phantom was developed to facilitate the study of LITT at 980nm in prostatic tissue. The thermal and optical properties of the phantom were designed to match human prostatic tissue. As a result, the thermal response of the phantom was consistent with that observed clinically. The induced coagulation zone can be observed directly or via T_2-weighted MRI. Furthermore, LITT-induced coagulation is both qualitatively and quantitatively similar to that observed in *in vivo* human prostate. This phantom provides a

useful platform for the development and optimization of LITT techniques including monitoring modalities such as interstitial probes and MRT.

Acknowledgements

Jessica Martinez, Samantha Mikaiel and Fuad Elkhoury assisted with the acquisition of MRI data.

References

1. Natarajan S, Raman S, Priester AM, Garritano J, Margolis DJA, et al. Focal Laser Ablation of Prostate Cancer: Phase I Clinical Trial. J Urol 2016; 196:68–75. [PubMed: 26748164]
2. Eggener SE, Yousuf A, Watson S, Wang S, Oto A. Phase II Evaluation of MRI-Guided Focal Laser Ablation of Prostate Cancer. J Urol 2016; 196:1670–1675. [PubMed: 27449263]
3. Oto A, Sethi I, Karczmar G, McNichols R, Ivancevic MK, et al. MR Imaging – guided Focal Laser Ablation for Prostate Cancer : Phase 1 Trial. Radiology 2013; 267:932–640. [PubMed: 23440319]
4. Lepor H, Llukani E, Sperling D, Futterer JJ. Complications, Recovery, and Early Functional Outcomes and Oncologic Control Following In-bore Focal Laser Ablation of Prostate Cancer. Eur Urol 2015; 68:924–926. [PubMed: 25979568]
5. Peters RD, Chan E, Trachtenberg J, Jothy S, Kapusta L, et al. Magnetic resonance thermometry for predicting thermal damage: An application of interstitial laser coagulation in an in vivo canine prostate model. Magn Reson Med 2000; 44:873–883. [PubMed: 11108624]
6. Stafford RJ, Shetty A, Elliott AM, Klumpp SA, McNichols RJ, et al. Magnetic resonance guided, focal laser induced interstitial thermal therapy in a canine prostate model. J Urol 2010; 184:1514–1520. [PubMed: 20727549]
7. van Nimwegen SA, L'Eplattenier HF, Rem AI, van der Lugt JJ, Kirpensteijn J. Nd:YAG surgical laser effects in canine prostate tissue: temperature and damage distribution. Phys Med Biol 2009; 54:29–44. [PubMed: 19060357]
8. Seitz M, Reich O, Gratzke C, Schlenker B, Karl A, et al. High-power diode laser at 980 nm for the treatment of benign prostatic hyperplasia: Ex vivo investigations on porcine kidneys and human cadaver prostates. Lasers Med Sci 2009; 24:172–178. [PubMed: 18270761]
9. Bomers JGR, Cornel EB, Futterer JJ, Jenniskens SFM, Schaafsma HE, et al. MRI-guided focal laser ablation for prostate cancer followed by radical prostatectomy: correlation of treatment effects with imaging. World J Urol 2016; 35:703–711. [PubMed: 27541586]
10. Lindner U, Weersink RA, Haider MA, Gertner MR, Davidson SRH, et al. Image guided photothermal focal therapy for localized prostate cancer: phase I trial. J Urol 2009; 182:1371–1377. [PubMed: 19683262]
11. Natarajan S, Jones TA, Priester AM, Geoghegan R, Lieu P, et al. Focal Laser Ablation of Prostate Cancer: Feasibility of Magnetic Resonance Imaging-Ultrasound Fusion for Guidance. J Urol 2017; 198:839–847. [PubMed: 28396184]
12. Jaywant S, Wilson B, Patterson M, Lilge L, Flotte T, et al. Temperature-dependent changes in the optical absorption and scattering spectra of tissues: correlation with ultrastructure In: Laser-Tissue Interaction IV.International Society for Optics and Photonics; 1993 pp. 218–229.
13. Nau WH, Roselli RJ, Milam DF. Measurement of thermal effects on the optical properties of prostate tissue at wavelengths of 1,064 and 633 nm. Lasers Surg Med 1999; 24:38–47. [PubMed: 10037350]
14. Skinner MG, Everts S, Reid AD, Vitkin IA, Lilge L, et al. Changes in optical properties of ex vivo rat prostate due to heating. Phys Med Biol 2000; 45:1375–1386. [PubMed: 10843110]
15. Niemz MH. Laser-Tissue Interactions: Fundamentals and Aplications. Third Berlin: Springer; 2007.
16. Nikfarjam M, Malcontenti-Wilson C, Christophi C. Comparison of 980- and 1064-nm Wavelengths for Interstitial Laser Thermotherapy of the Liver. Photomed Laser Surg 2005; 23:284–288. [PubMed: 15954816]

17. Jiang SC, Zhang XX. Dynamic modeling of photothermal interactions for laser-induced interstitial thermotherapy : parameter sensitivity analysis. Lasers Med Sci 2005; 20:122–131. [PubMed: 16328097]
18. Negussie AH, Partanen A, Mikhail AS, Xu S, Abi-Jaoudeh N, et al. Thermochromic tissue-mimicking phantom for optimisation of thermal tumour ablation. Int J Hyperthermia 2016; 32:239–243. [PubMed: 27099078]
19. Bu-Lin Z, Bing H, Sheng-Li K, Huang Y, Rong W, et al. A polyacrylamide gel phantom for radiofrequency ablation. Int J Hyperthermia 2008; 24:568–576. [PubMed: 18608575]
20. McDonald M, Lochhead S, Chopra R, Bronskill MJ. Multi-modality tissue-mimicking phantom for thermal therapy. Phys Med Biol 2004; 49:2767–2778. [PubMed: 15285246]
21. Bouchard LS, Bronskill MJ. Magnetic resonance imaging of thermal coagulation effects in a phantom for calibrating thermal therapy devices. Med Phys 2000; 27:1141–1145. [PubMed: 10841421]
22. Hills BP, Takacs SF, Belton PS. The effects of proteins on the proton N.M.R. transverse relaxation time of water II. Protein aggregation. Mol Phys 1989; 67:919–937.
23. Iizuka MN, Sherar MD, Vitkin IA. Optical phantom materials for near infrared laser photocoagulation studies. Lasers Surg Med 1999; 25:159–169. [PubMed: 10455223]
24. Takada J, Honda N, Hazama H, Awazu K. Ex vivo evaluation of safety and efficacy of vaporization of the prostate using a 300 W high-power laser diode with the wavelength of 980 nm. Laser Ther 2014; 23:165–172. [PubMed: 25368442]
25. Roggan A, Albrecht HJ, Doerschel K, Minet O, Mueller GJ. Experimental setup and Monte-Carlo model for the determination of optical tissue properties in the wavelength range 330-1100nm. In: Proc. SPIE 2323Berlin: International Society for Optics and Photonics; 1995 pp. 21–36.
26. Flock ST, Jacques SL, Wilson BC, Star WM, Van Gemert MJC. Optical properties of intralipid: A phantom medium for light propagation studies. Lasers Surg Med 1992; 12:510–519. [PubMed: 1406004]
27. van Staveren HJ, Moes CJM, van Marie J, Prahl SA, van Gemert MJC. Light scattering in lntralipid-10% in the wavelength range of 400–1100 nm. Appl Opt 1991; 30:4507–4514. [PubMed: 20717241]
28. Welch AJ, van Germert MJC, Van Gemert MJC. Optical-thermal response of laser-irradiated tissue. New York: Springer; 2011.
29. Shrake A, Ross PD. Origins and consequences of ligand-induced multiphasic thermal protein denaturation. Biopolymers 1992; 32:925–940. [PubMed: 1420977]
30. Ahmad N, Qasim MA. Fatty Acid Binding to Bovine Serum Albumin Prevents Formation of Intermediate During Denaturation. Eur J Biochem 1995; 227:563–565. [PubMed: 7851438]
31. Cubeddu R, Pifferi A, Taroni P, Torricelli A, Valentini G. A solid tissue phantom for photon migration studies. Phys Med Biol 1997; 42:1971–1979. [PubMed: 9364593]
32. Ninni P Di, Martelli F, Zaccanti G. Effect of dependent scattering on the optical properties of Intralipid tissue phantoms. Biomed Opt Express 2011; 2:2265–2278. [PubMed: 21833363]
33. Royston DD, Poston RS, Prahl SA. Optical Properties of Scattering and Absorbing Materials Used in the Development of Optical Phantoms at 1064nm. Biomed Opt Express 1996; 1:110–116.
34. Prahl SA. Everything I think you should know about inverse adding-doubling. Oregon Med Laser Center, St Vincent Hosp 2011; :1–74.
35. Geoghegan R, Priester A, Lieu P, Macarian ML, Pantuck A, et al. Determining Optimal Exposure Duration for Focal Laser Ablation of the Prostate. In: Proceedings of the 31st Annual Meeting of the Engineering & Urology SocietySan Diego: ; 2016.
36. Jiang SC, Zhang XX. Effects of dynamic changes of tissue properties during laser-induced interstitial thermotherapy (LITT). Lasers Med Sci 2005; 19:197–202. [PubMed: 15647970]
37. Dabbagh A, Abdullah BJJ, Kasim NHA, Ramasindarum C. Reusable heat-sensitive phantom for precise estimation of thermal profile in hyperthermia application. Int J Hyperth 2014; 30:66–74.

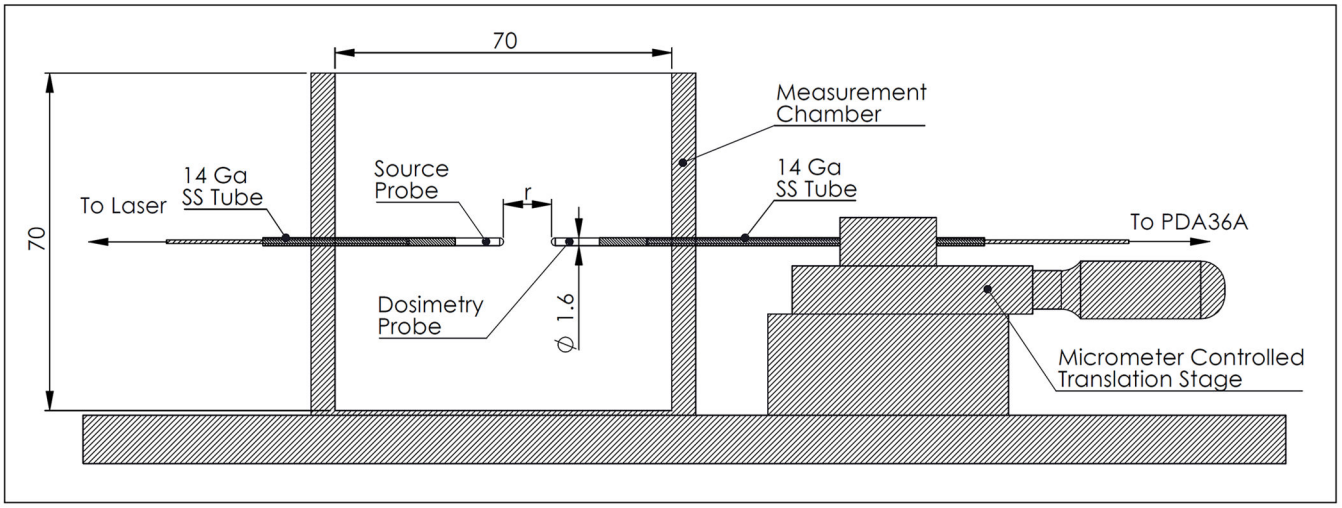

Fig. 1:

Apparatus used to quantify μ_s'. Phantoms were cast in 70mm x 70mm x 40mm thin walled (1mm) containers with holes for the source and dosimetry probes. During testing the container holding the phantom is placed in the measurement chamber before inserting the probes.

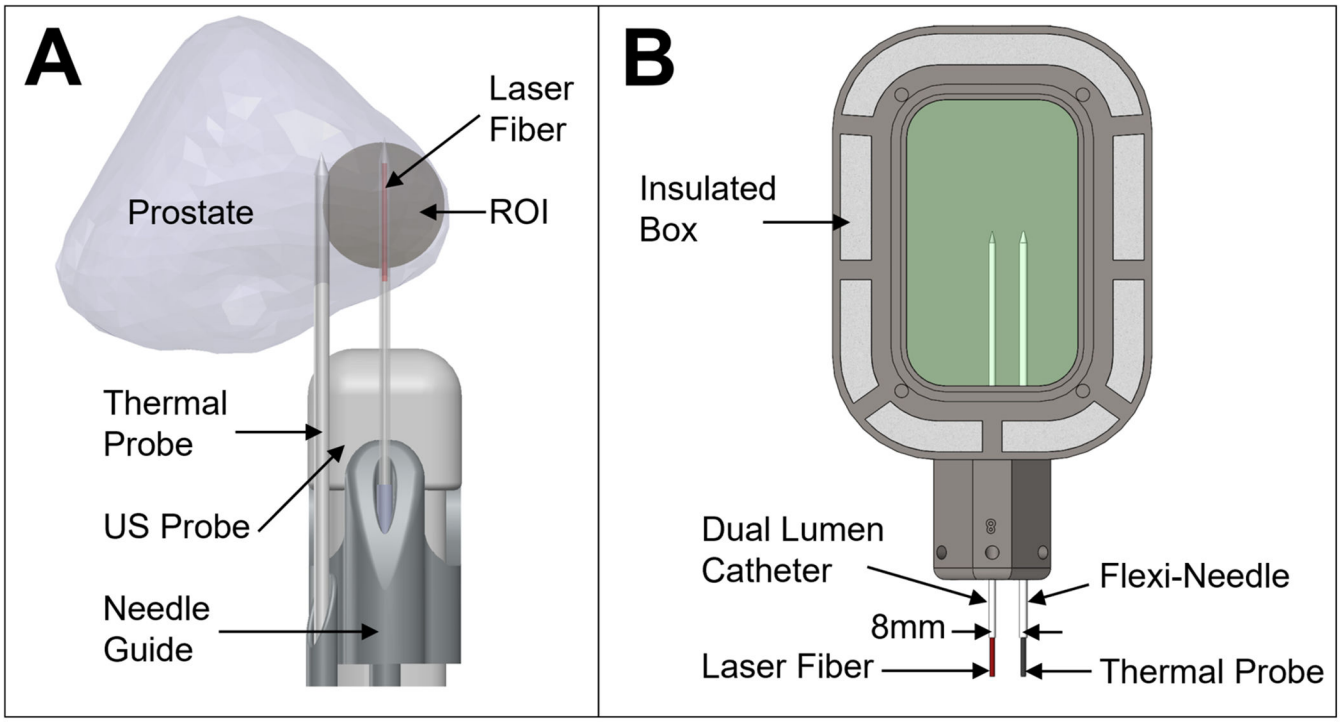

Fig. 2:

A) Clinical setup during MR-US fusion guided LITT for the treatment of prostate cancer. LITT was performed in the region of interest (ROI) for 3 min. at 13.75W with a 980nm laser. A thermal probe was used to record temperature. B) Experimental setup mimicking clinical conditions. The phantom was heated to 37°C in a water bath prior to being placed in the insulated box. LITT was performed using the same equipment and configuration used clinically.

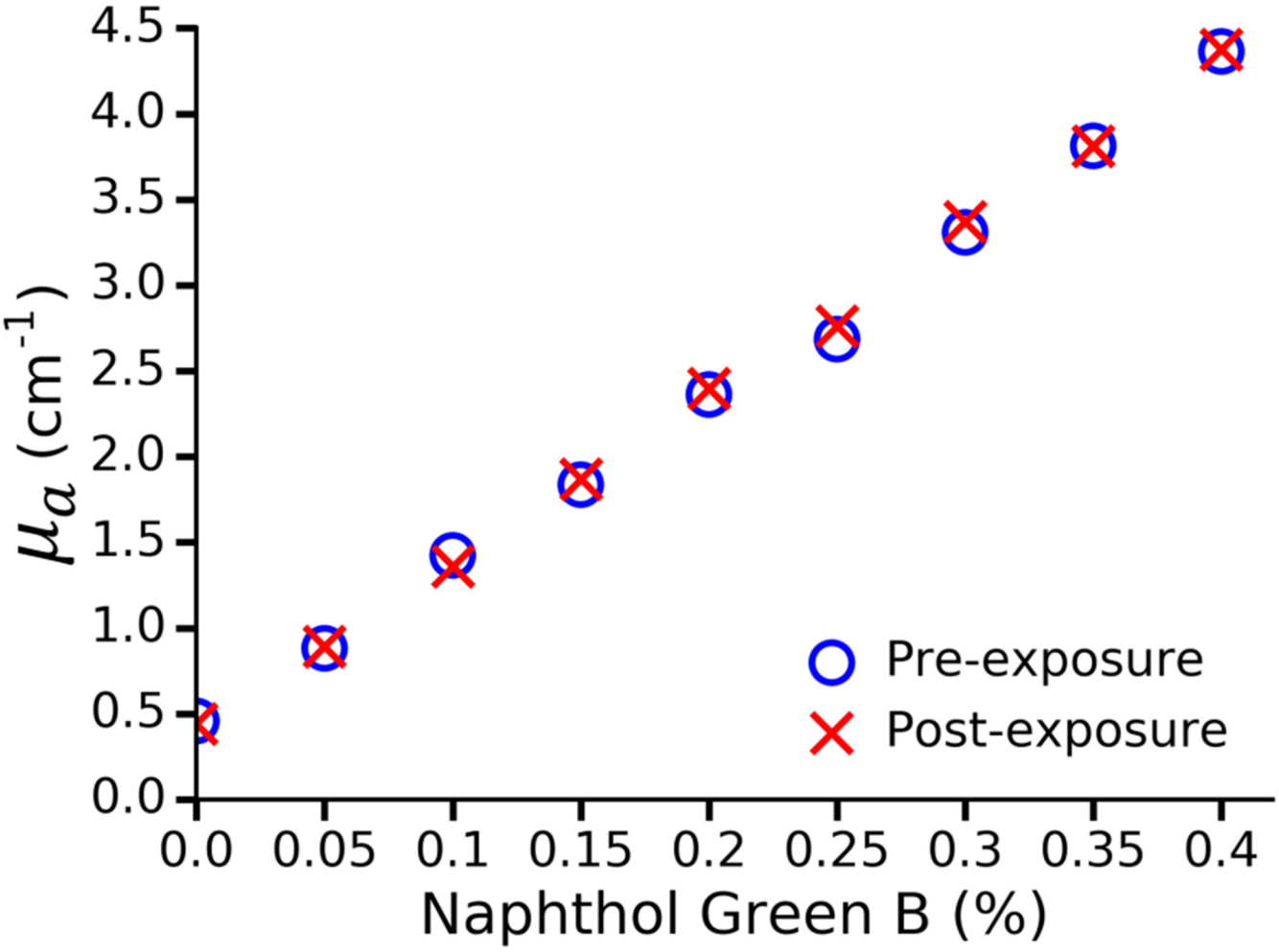

Fig. 3:
The effect of photobleaching in Naphthol Green B/water solutions at 980nm. No change was observed as a result of laser exposure.

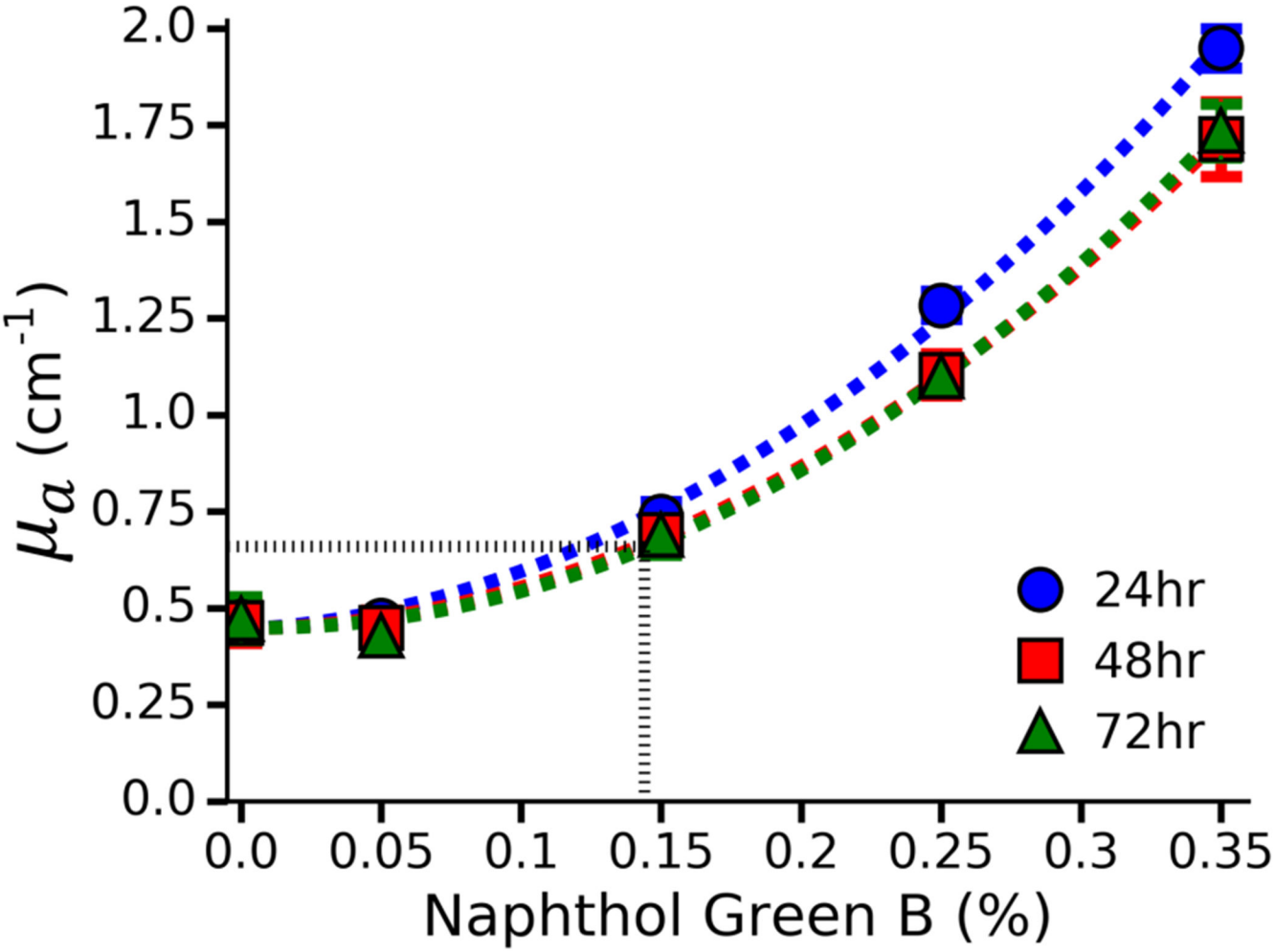

Fig. 4:

μ_a as function of Naphthol Green B concentration at 980nm in polyacrylamide gel. μ_a was determined by a spectrophotometer at 24, 48 and 72 hours. No further bleaching was observed after 48 hours. By interpolation (dashed black line), a 0.144% concentration of Naphthol Green B was found to provide the desired μ_a of 0.66 ± 0.06 cm^{-1}.

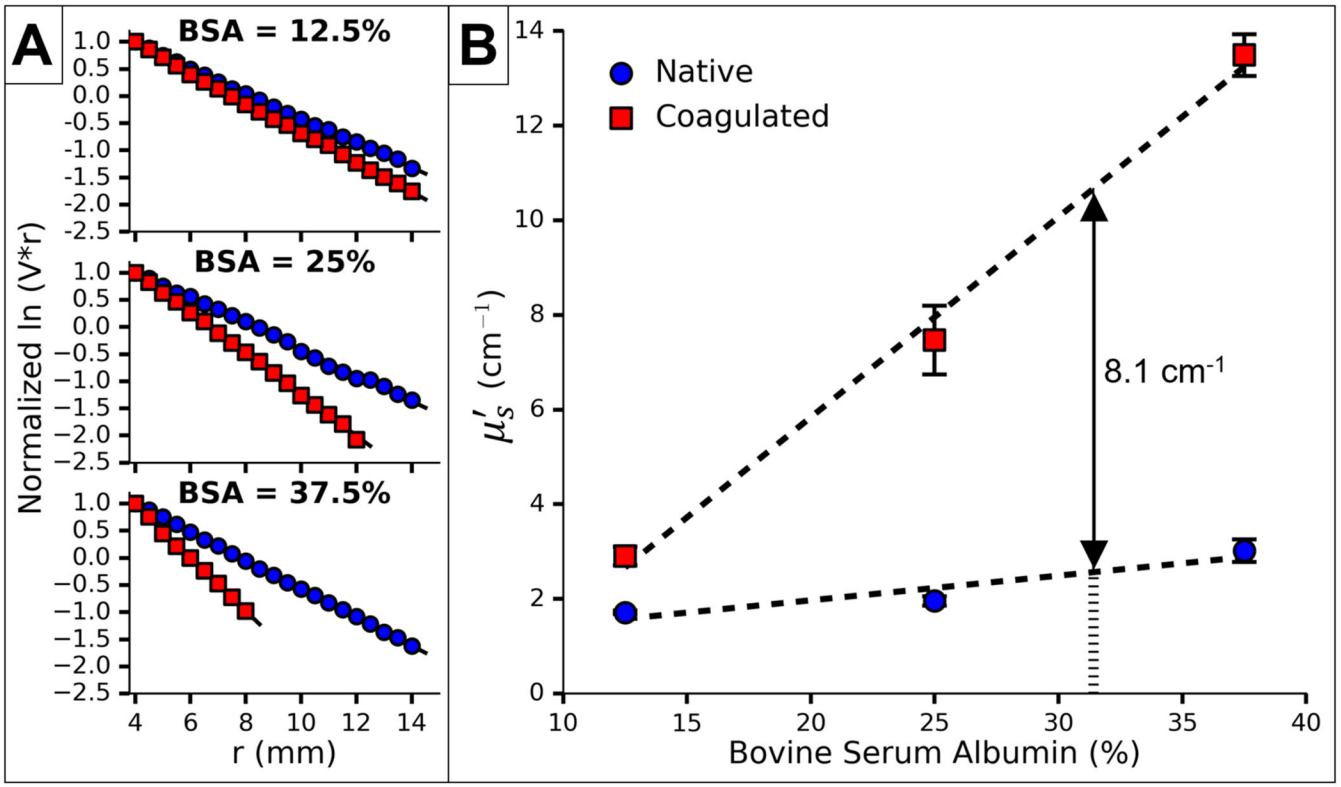

Fig. 5:

A) Normalized $ln\,(V \cdot r)$ vs r for a single set of phantoms doped with 12.5%, 25% and 37.5% BSA and 0.144% Naphthol Green B. B) The effect of BSA concentration on μ_s' before and after coagulation measured in 3 sets of phantoms. Given the desired coagulation-induced change in μ_s' of 8.1cm^{-1}, the requisite concentration of BSA was found to be 31.4%. Error bars represent one standard deviation and are not visible at all points.

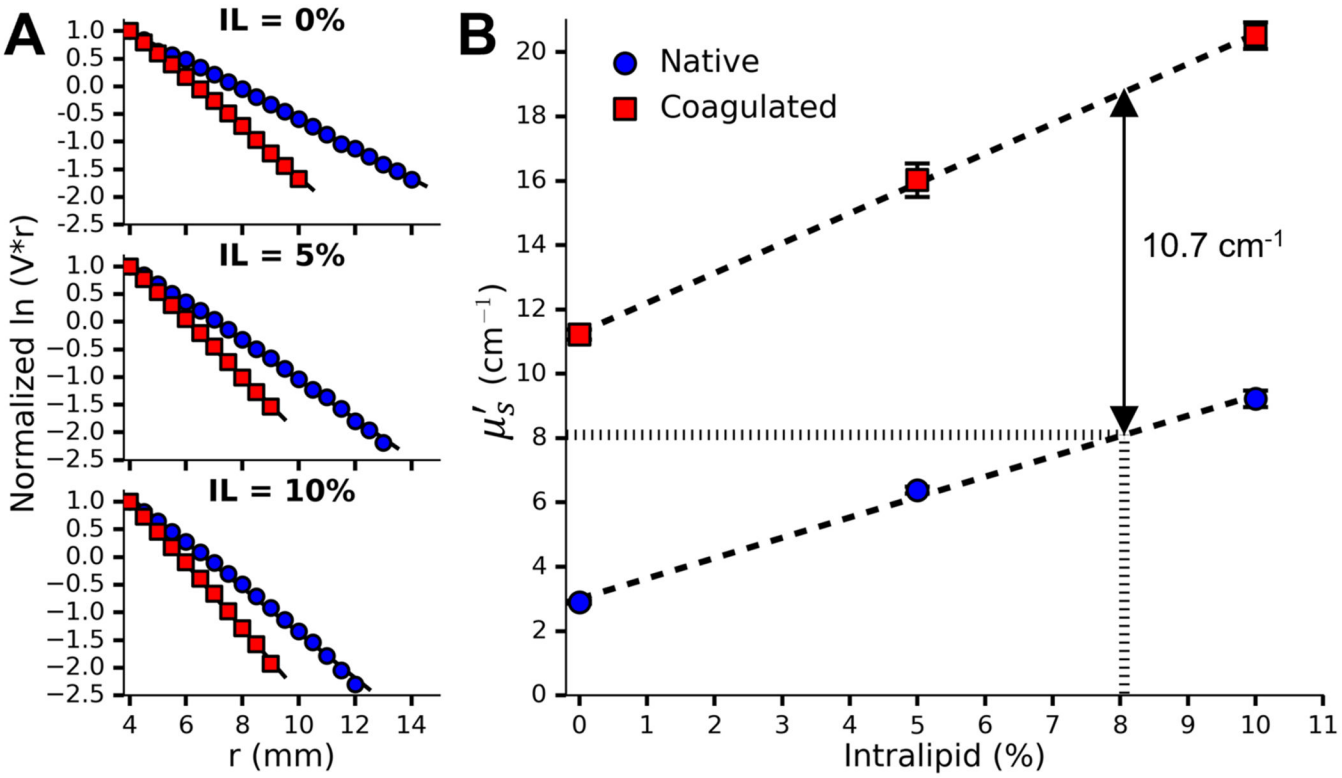

Fig. 6:

A) Normalized $ln\,(V \cdot r)$ vs r for a single set of phantoms doped with 0%, 5% and 10% Intralipid, 0.144% Naphthol Green B and 31.4% BSA. B) The effect of Intralipid and BSA concentration on μ_s' before and after coagulation measured in 3 sets of phantoms. By interpolation, the requisite concetraion of Intralipid was found to be 8.06%. Error bars represent one standard deviation and are not visible at all points.

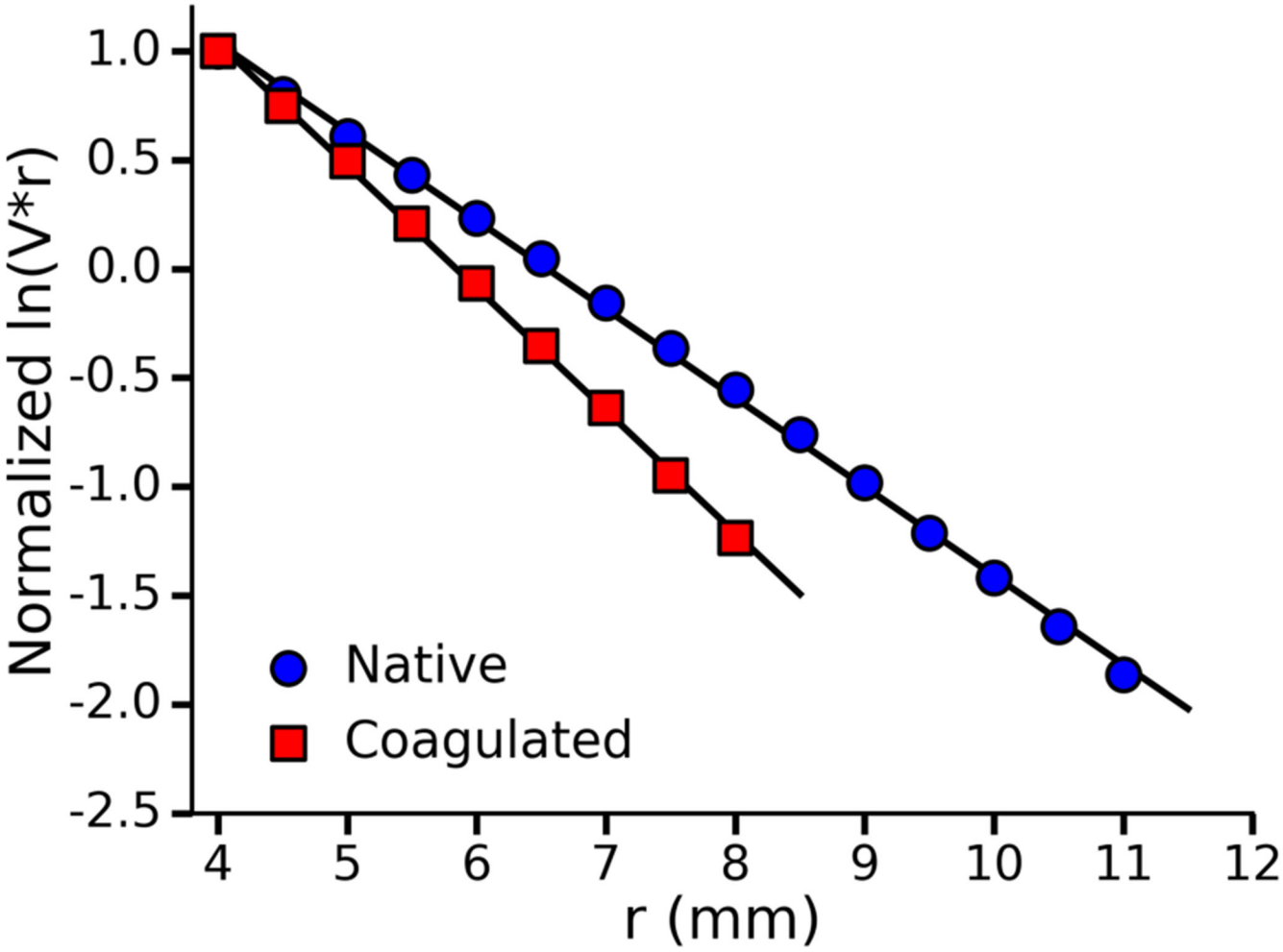

Fig. 7:

Normalized ln(V.r) vs r for a single optimized phantom before and after coagulation. A total of five phantom were tested and one standard deviation was used to quantify the uncertainty in the measured optical properties shown in Table 3

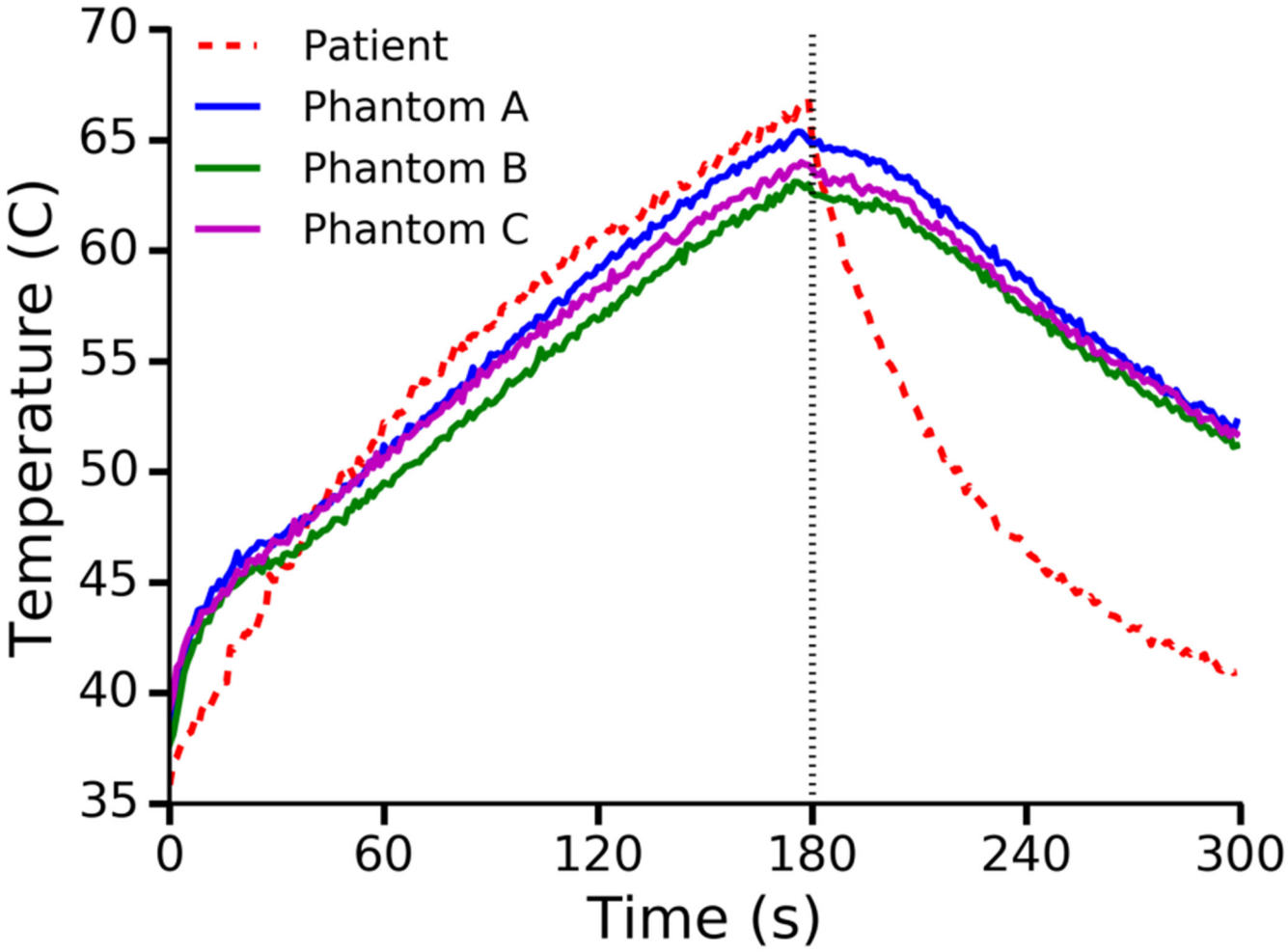

Fig. 8:

Temperature at a radial distance of 8mm from the laser as measured in a patient and three phantoms. Dashed black line indicates laser deactivation.

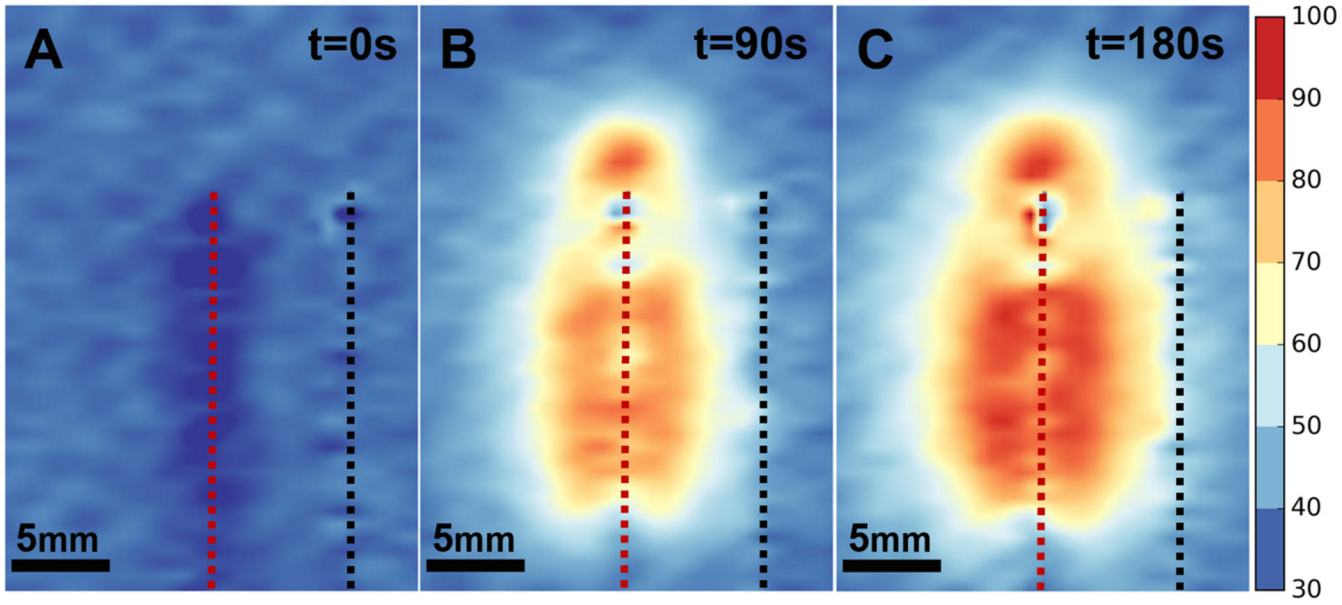

Fig. 9:

Absolute temperature (°C) during LITT of the optimized phantom as determined by MRT at 0 (A), 90 (B) and 180 (C) seconds after laser activation. The location of the laser fiber (dashed red line) and thermal probe (dashed black line) are marked

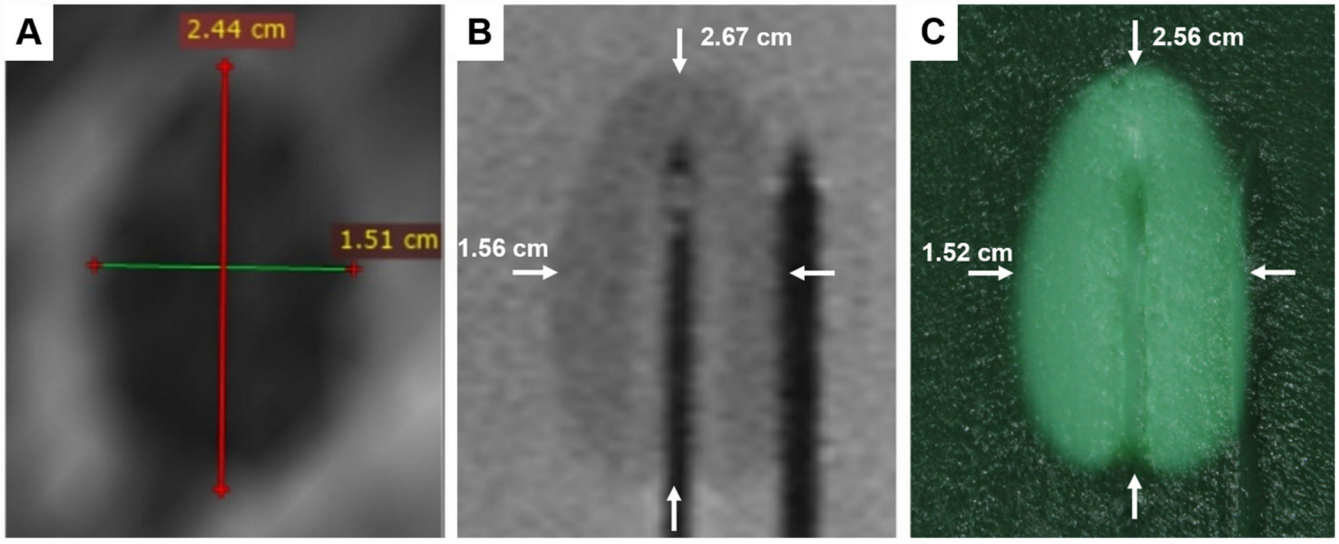

Fig. 10:

A) Zone of coagulative necrosis in a patient as indicated by non-perfused tissue. The scan was acquired immediately after the patient received LITT for 3 min. at 13.75W. Further information can be found in Natarajan et al. (2017)[11]. B) Phantom coagulation zone under T_2-weighted MRI showing major and minor axes (white arrows). Note that the catheters in the center and on the right contain the laser fiber and thermal probe respectively. C) Phantom coagulation zone under direct visualization showing major and minor axes (white arrows). Note the needle tracks in the center and to the right.

Table 1:

Phantom recipe without altering optical properties (1L)

Ingredients	Dosage
Acrylamide/Bis-acrylamide (40% w/v)	250ml
Deionized water	744.5ml
Citric Acid Anhydrous	17.063g
Sodium Citrate Tribasic Dihydrate	32.696g
Initiator-Activator	
L-ascorbic acid	1g
$FeSO_4$ (1% w/v)	2.5ml
Hydrogen Peroxide (3% v/v)	3ml

Table 2:

Tissue-mimicking phantom recipe (1L)

Ingredients	Dosage
Acrylamide/bis-acrylamide (40% w/v)	250ml
Deionized water	349.9ml
Naphthol Green B	1.44g
Intralipid (20%)	80.6ml
BSA (30.6%)	314ml
Citric Acid Anhydrous	17.063g
Sodium Citrate Tribasic Dihydrate	32.696g
Initiator-Activator	
L-ascorbic acid	1g
$FeSO_4$ (1% w/v)	2.5ml
Hydrogen Peroxide (3% v/v)	3ml

Table 3:

Optical properties of tissue-mimicking phantom

	μ_a (cm^{-1})	μ_s' (cm^{-1})
Native	0.66 ± 0.06	8.27 ± 0.50
Coagulated	0.66 ± 0.06	17.63 ± 1.41